Hindawi
Advances in Materials Science and Engineering
Volume 2020, Article ID 1732621, 11 pages
https://doi.org/10.1155/2020/1732621

Research Article

The Mechanism of the First Hydration-Dehydration Cycle of Pure α- and β-$CaSO_4 \cdot 0.5H_2O$

E. Abu Zeitoun,[1] **C. Pritzel**,[1] **Y. Sakalli**,[2] **and R. Trettin**[1]

[1]*Institute of Building and Materials Chemistry, University of Siegen, Paul-Bonatz-Str. 9-11, Siegen, Germany*
[2]*Micro- and Nanoanalytics Facility, University of Siegen, Paul-Bonatz-Str. 9-11, Siegen, Germany*

Correspondence should be addressed to E. Abu Zeitoun; abuzeitoun@chemie.uni-siegen.de

Received 13 March 2020; Revised 14 May 2020; Accepted 11 June 2020; Published 3 July 2020

Guest Editor: Kestutys Baltakys

The objective of this research was to understand the dehydration mechanism of technical dihydrate and the variation of the physical properties of β-hemihydrate after the first hydration-dehydration process. In this study, the recycling mechanism of different hemihydrate types as raw material was investigated. The influence of the first hydration-dehydration process on the hydration rate, microstructure, and mechanical properties of recycled hemihydrate were characterized by differential calorimetric analysis (DCA), calcium ion-selective electrode (Ca^{2+}-ISE), conductivity, particle size distribution (PSD), scanning electron microscopy (SEM), and X-ray diffraction (XRD). The results showed that the formed hemihydrate after the first hydration-dehydration process differs in its properties than the unrecycled hemihydrate in some characteristics such as the morphological structure, number of surface, and side defects due to the grinding process after the first hydration step. In addition to the grinding step, the calcination process was responsible for increasing the number of defects on the crystal surface, which leads to a change in setting time and the microstructure of the recycled hemihydrate. Therefore, after the 1st reaction cycle of β-HH, the compressive strength decreases due to a decrease in the hemihydrate crystal size, an increase in the surface area, and an increase in the amount of water required to perform the hydration reaction. The obtained hemihydrate after the first hydration-dehydration process was in β form due to the applied calcination process after the first cycle.

1. Introduction

Calcium sulfate hemihydrate plaster is considered one of the most popular sustainable binders used in the construction industry due to low production energy, low market price, fire-resistant, and good thermal properties [1–5]. It is commonly used as an ingredient in paste and mortar plastering and production of some building components such as plasterboards and building blocks. Moreover, it can be used as an additive in polymers, cement, and food industries [1, 3, 6–11]. The annual production of calcium sulfate-based binders is more than 260 million tons worldwide, of that, over 80 million tons are applied in the production of gypsum plasterboards. The obtained gypsum can be founded either naturally or industrially as a byproduct [12–14]. The flue gas desulfurization process (FGD) delivers over one-half of this binder to the industrial sectors [15, 16]. However, this source will not exist in the future due to the need for energy conservation and sustainable methods of production. Therefore, it is useful to recycle gypsum waste and consider the recycled material as an alternative resource to be used in cement, building, and ceramic industries [3–5, 11, 17–19]. The construction and demolition (CD) processes are considered as one of the largest contributors to waste in the world. Moreover, the obtained gypsum plaster waste from construction and demolition processes accumulates to 15 million tons annually [4, 20, 21]. One of the common destinations for these wastes is landfilling. However, it is feasible to develop a new technology to reuse these wastes in further applications due to limited space and contaminating groundwater sources in addition to the environmental regulation of some countries. It has been reported that gypsum plasterboard wastes can be recycled in a sequential process by crushing, separating, and

burning to transform the dihydrate into the hemihydrate phase [17]. According to their report, it is useful as geomaterial or ground improvement material due to its effectiveness in many engineering and economic aspects [17]. The conversion of gypsum into a recycled product has been interesting for many researchers due to its reaction reversibility, cycle-ability, stability, environmental safety, nontoxicity, and sustainability [4, 11, 18, 19, 22]. In this study, the pure β- and SA α-HH were recycled one time by applying similar calcination conditions in an attempt to understand the dehydration mechanism in detail. Furthermore, the changes in physiochemical properties of the newly generated hemihydrate were studied.

1.1. Experimental Procedure. In the first step, the cycling process was defined by hydration-dehydration process and considered as the first reaction cycle, because alpha- and beta hemihydrate were the starting material in the cycling process. The chemical composition of alpha hemihydrate (α-HH) from the steam autoclave process and beta hemihydrate (β-HH) were determined by XRD as shown in Table 1. In more detail, hemihydrate was added to water to perform the hydration reaction to obtain dihydrate, and then, the formed dihydrate was crushed and calcinated back to beta hemihydrate. The stoichiometric amount of water needed for hydration is around 15.7 ml per 100 g, but an excess amount of water is required to obtain gypsum slurry with good workability. Therefore, the rheological test is very important to determine the water to solid (*w/s*) ratio for any hemihydrate type individually since it is a function of particle size [22, 23]. Figure 1 represents the cycling mechanism of gypsum, starting from hemihydrate. In the first stage, the hydration reaction will take place immediately after hemihydrate addition to water. The hydration time varies depending on the physical properties of the hemihydrate used in this process. After the hydration is completed, the excess amount of water needs to be evaporated to achieve the mechanical strength of the dihydrate crystals. In the second stage, the calcination of the formed dihydrate crystals was performed at 140°C for at least 4 hours to ensure the complete dehydration of dihydrate.

Deionized water was used for all liquid phases. For the rheological test, 100 g of hemihydrate was added to water and mixed for 1 minute. The mix was filled into a hollow cylinder (inner diameter 30 mm and height 50 mm), which was placed on a glass plate, and then the cylinder was pulled up vertically. The glass plate was removed up and down five times by rotating a special handle attached to the stage clockwise in order to disperse the collapsed mix. The average of three perpendicular diameters of the dispersed slurry was defined as slump flow. The reaction kinetic was performed by differential calorimetric analysis (DCA) (Toni Technik Baustoffprüfsysteme GmbH-Germany) using (1 : 1) water to solid ratio. The measurement time and temperature were fixed at 24 hours and 25°C, respectively. From this measurement, the heat rate during the hydration was monitored, as well as the total heat released [24]. The calcium concentration was carried out by Ca-ion-selective electrode (ISE) (Mettler-Toledo GmbH-Germany). The samples were prepared according to gypsum solubility. Prior to each measurement, the Ca^{2+}-ISE was calibrated to ensure the electrode efficiency. Both electrodes (Ca^{2+}-ISE and conductivity electrode) were immersed in 200 ml deionized water to record the blank value before the addition of 3.2 g of hemihydrate. The changes in calcium concentration and reaction conductivity were recorded every 30 seconds for four hours at 20°C [25]. Particle size distribution was detected by Mastersizer 2000, Malvern Instruments GmbH-Germany. Before starting the measurement, the sample chamber was rinsed and filled with isopropanol; then, a small amount of the powdered sample was added to the sample chamber at a stirring speed of 2000 rpm to ensure sample delivery to the measuring cell. The amount of sample was controlled by the so-called obscuration range of the laser beam, which should lie between 10 and 20% according to the user manual of the instrument [26]. The specific surface area of powder was determined by the physical adsorption of a gas on the surface of the solid using the BET method (Micromeritics ASAP2020 (Micromeritics GmbH)) [27, 28]. Both quantitative and qualitative analyses of hemihydrate samples were measured using XRD. Rietveld refinement was used to analyze the samples quantitatively. The powder samples were filled in the XRD sample holders and transferred to the instrument; then the XRD pattern was taken using a Panalytical *x'pert pro* diffractometer with a Cu Kα source operated at 40 kV and 40 mA. The range of 2θ was between 8° and 40° [29]. The morphology of the formed crystals was recorded by scanning electron microscopy (Quanta 250 FEG, FEI GmbH-Germany). To perform the measurement, the sample has to be glued on the sample holder of the SEM using either a carbon conductive tab or silver paint. Samples were prepared without pretreatment and results with high resolution were obtained [30]. To monitor the dehydration of the generated dihydrate before and after the first reaction cycle, a Simultaneous Thermal Analysis (STA) method was utilized (STA 449 Netzsch GmbH-Germany) at N_2 atmosphere with a gas flow of 20 ml/min. This device consists of the thermal gravimetry (TG) and differential scanning calorimetry (DSC) apparatus fused into one system with the sole purpose of obtaining vital information from the thermal events recorded in the investigation of the sample over time [6]. The time of dehydration can be determined with this method as well as the mass loss caused by dehydration at certain temperatures. To measure the water release of dihydrate, a small amount of dihydrate powder was placed in a platinum crucible and heated in the STA at 10 K/min.

2. Results and Discussion

In the beginning, the first reaction cycle starts with hemihydrate; therefore, this step is called the hydration-dehydration process. The impact of this process on hydration kinetic and calcium concentration changes was measured. Figure 2(a) shows the comparison in the heat rate between the pure β-HH and the same hemihydrate after the 1st reaction cycle. The heat rate of the recycled β-HH is slower

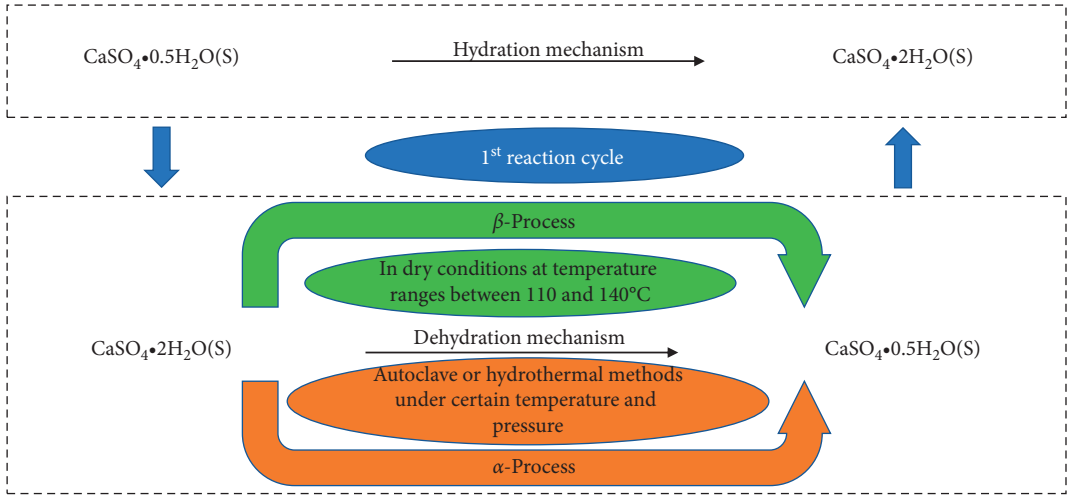

Figure 1: The mechanism of the 1st reaction cycle [17, 31].

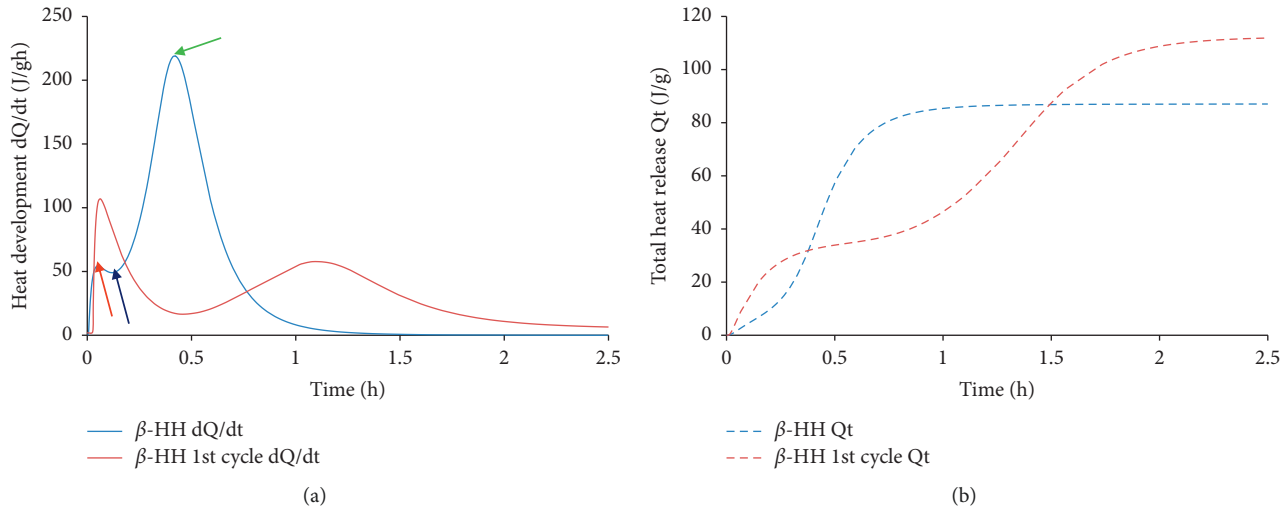

Figure 2: (a) Heat evolution curves and (b) total heat release of pure β-HH β-HH after 1st cycle.

than the pure β-HH due to the agglomeration of the hemihydrate particle which might hinder the solving of hemihydrate. In addition to the heat development changes, the total heat release in J/g was also measured during the recycling of β-HH, as shown in Figure 2(b). To verify that, the calcium ion concentration changes were measured during the hydration process.

The hydration reaction of β-HH before and after the 1st reaction cycle can be divided into four steps, as shown from the heat development curve in Figure 2(a). The first peak represents two hydration steps; in the first step, the hemihydrate becomes humidified, and a water film will be generated around the particles. This is followed by the solving process of the hemihydrate which should be exothermal because the solubility of hemihydrate has an inverse relation with temperature [12, 32, 33]. This results in the initial increase in heat development. The variation between pure β-HH and β-HH after the 1st reaction cycle in the first peak of the heat development was due to the presence of finer HH particle of the recycled material, as shown from d_{10} and d_{50} in Table 2. Through the rapid solving of hemihydrate, the ions concentration increases rapidly until they reach the start supersaturation denoted in Figure 2(a) with the red arrow. In the next step, after reaching the supersaturation, the hydration energy decreases up to the point indicated by the blue arrow because of seed crystal formation. During this time period, both processes (solving and seeds formation) takes place. The amount and rate of seeds formation depend highly on the ion concentration generated from the solving process. It is very important to note that the supersaturation is the driving force behind seeds formation. Moreover, the higher the ion concentration in the reaction solution, the more seeds are generated [34, 35].

The second peak of the heat development curve also represents two hydration reaction steps. In the beginning, the reaction energy increases again due to the continuous solving of the hemihydrate without the formation of new seeds. In the period which lies between the blue and green

arrows, only solving the remaining hemihydrate, in addition to the growing of the created seeds from the previous step, takes place. In the last step, which is the retardation period, most of the hemihydrate is consumed and the solving process delivers insufficient ions for the dihydrate crystals to be grown. At this point, when the ions concentration is around the solubility of dihydrate, then hydration stops [12]. The purity of hemihydrate, as well as the milling process, plays an important role during its hydration. The existence of any dihydrate crystals changes the whole hydration process. Therefore, the purity of hemihydrate before and after the 1st reaction cycle was analyzed quantitatively using XRD as illustrated in Table 1.

As shown in Figure 3, a similar behavior as the heat rate development was observed. In the beginning, the solving of β-HH after the first cycle was similar to the uncycled β-HH, and then the dissolution rate varies due to the agglomeration that is generated from the hydration-dehydration process. The previous investigation of the pure β-HH displayed that the surface area and the numbers of defects were responsible for the hydration rate neglecting the effect of agglomeration. Hence, when the agglomeration of the particles increases, the hydration rate will be affected, as shown from the DCA and Ca^{2+}-ISE results in Figure 3. In order to explain that in detail, surface area and particle size distribution measurements were carried out. After the reaction cycle, two maxima of the particle size distribution were observed, as shown in Figure 4. This represents the formation of fine crystal d_{10} and d_{50} values in addition to an agglomeration of these crystals together with d_{90} value. As illustrated in Figure 3, at the beginning of the hydration, the ion delivery rate of the recycled β-HH was higher than the pure β-HH due to the generation of finer hemihydrate crystals after the 1st reaction cycle as presented form d_{10} and d_{50} values in Table 2 since the finer the particle size, the higher the rate of ion delivery. Therefore, the maximum supersaturation and conductivity of the recycled β-HH are higher than the pure β-HH, as shown in Figure 3. After a while, once the whole recycled β-HH fine crystals are dissolved, the hydration rate was retarded in comparison to the pure hemihydrate, as shown from DCA, Ca^{2+}-ISE, and conductivity measurements due to the agglomeration that is generated from the hydration-dehydration process as shown in Figure 4.

Table 2 summarizes the particle size distribution with surface area changes. The surface area increases after the first reaction cycle, and this implies that the size of the crystal decreases, as shown from d_{10} and d_{50} values. Figure 5 represents the SEM images of the pure β-HH and β-HH after the 1st cycle before and after four hours of hydration.

The crystal morphology differences between the pure β-HH and β-HH after the first cycle before hydration represent the generation of a fine hemihydrate crystal with agglomeration. After four hours of in situ hydration, SEM images were taken to view the morphology of the dihydrate crystals. As shown in Figure 5, the formed dihydrate crystals after the first cycle have the same crystal morphology as the formed dihydrate crystal from the pure hemihydrate before cycling. The differences in the physical properties, as shown from Table 2, have a large effect on the required amount of water which is needed to achieve good workability as well as the mechanical properties. The w/s ratio was determined according to a certain slump flow in the range of 82–85 mm.

The changes in crystal morphology and particle size lead to a variation in the mechanical properties. Therefore, the compressive strength for the pure β-HH and β-HH after one cycle was measured and calculated, as shown in Figure 6. The drop in the compressive strength after the first reaction cycle was due to the significant increase in the w/s ratio from 0.8 to 1 and the changes in the microstructure.

Regarding this change in the compressive strength, both pore radius and the microstructure development were measured by Mercury porosimetry and SEM, respectively. The pore radius size increases from 0.76 to 1.97 μm. Furthermore, the voids between the dihydrate crystals after one cycle increase, as shown in Figure 7. Hence, the formed β-HH after the first hydration-dehydration process differs in its properties than the unrecycled β-HH due to the grinding process after the first hydration step. So, the grinding step beside the dehydration process of the recycled material decreases the particle size, increases the surface area, and changes the microstructure. The finer the particle size, the higher the amount of required water to perform better workability leading to a decrease in the compressive strength of the recycled hemihydrate. In addition, the grinding step increases the number of defects on the crystal surface, which leads to a change in the set time and the microstructure of the recycled hemihydrate. The only way to get a hemihydrate slurry with the needed workability is the usage of a superplasticizers, but those additives are influencing the hydration behavior of the hemihydrate and the morphology of the formed dihydrate crystals [36, 37]. That was the reason to keep the workability constant by adding more water. With a constant amount of water, mixing of the hemihydrate slurry was impossible.

From the XRD results obtained, the phase composition of both types of hemihydrates has no significant changes after the 1st reaction cycle, as shown in Table 1. This indicates that the hemihydrate was well dehydrated at 140°C as no dihydrate phase was discovered. The impurities which were presented before cycling remain unchanged. Commonly known impurities in gypsum are usually in the form of carbonates, silica, or soluble salts. These impurities varied depending on the mine source of gypsum [12, 13, 38].

The same hydration-dehydration process was applied to the SA α-HH. After the hydration of SA α-HH, the obtained dihydrate was calcined in a dry atmosphere at 140°C for four hours. Therefore, the obtained hemihydrate after the first hydration-dehydration process was in β form. Different properties, such as the particle size, specific surface area, and w/s ratio, were evaluated as shown in Table 3. The applied calcination condition on the obtained dihydrate was mainly responsible for the variation in the physical properties between the SA α-HH and the HH after the 1st reaction cycle.

The rate of change of calcium concentration and ion conductivity over time for SA α-HH and SA α-HH after the first cycle was recorded. As shown in Figure 8, the calcium ion concentration rate for SA α-HH after one cycle became faster than the uncycled sample. The ion conductivity

Table 1: Chemical composition of pure β-HH and SA α-HH before and after the first cycle.

Chemical composition (%)	Quartz	Anhydrite II	Hemihydrate	Dihydrate	Syngenite	Calcite
β-HH	0.3	2.1	94.3	1.8	0.2	1.3
β-HH-1st cycle	0.5	3.4	94.6	0.0	0.2	1.3
SA α-HH	0.6	0.7	97.3	0.0	0.3	1.0
SA α-HH 1st cycle	1.0	1.1	96.1	0.1	0.3	1.3

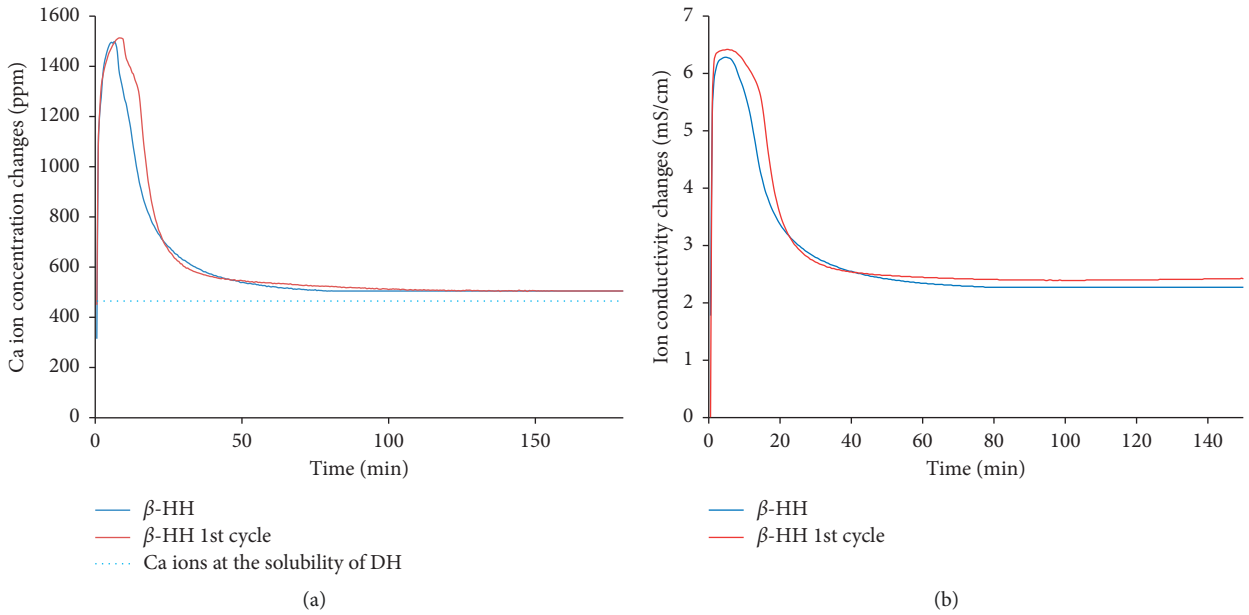

Figure 3: Ca^{2+}-Ion concentration and ion conductivity changes for pure β-HH and β-HH after the first cycle: (a) ion concentration changes and (b) ion conductivity changes.

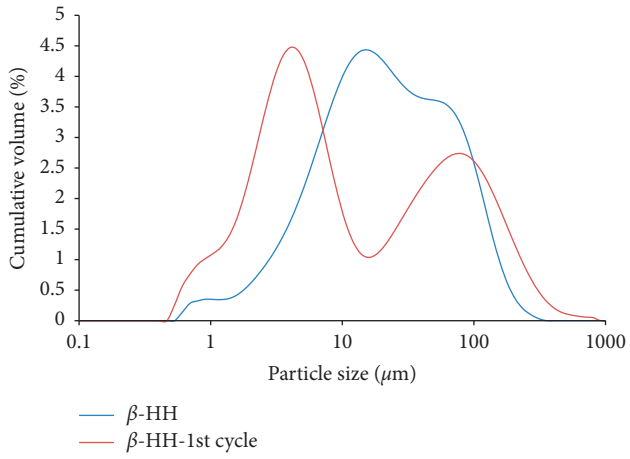

Figure 4: Particle size distribution of pure β-HH and β-HH after the first cycle.

changes maintain similar behavior like calcium ion changes. The main reason for such changes was the grinding process in addition to the applied calcination condition after the hydration-dehydration process of the SA α-HH. The original SA α-HH has large particles with nearly a smaller number of defects on its crystal surfaces, but due to the grinding process, the crystal size decreases, and the number of defect positions on the outer surface of each crystal increases. The particle size distribution becomes smaller during the recycling processes with less agglomeration compared to the pure SA α-HH, as shown in Figure 9. Therefore, the surface area and the hydration rate of SA α-HH were significantly increased. The pure SA α-HH has a slower heat rate changes than its recycled sample because of the large difference between the sample before and after cycling since the generated hemihydrate is in a β form not in α form due to the applied calcination condition during the first recycling step.

The recycled β-HH had shown retardation in its rate of calcium ion concentration and ion conductivity changes in contrast to the unrecycled β-HH, whereas the generated hemihydrate after the first hydration-dehydration process of SA α-HH had shown a rapid change in its rate of calcium ion concentration and ion conductivity as illustrated in Figure 8. The reason is due to differences in the crystal morphology between the started hemihydrate types and the impact of recycling and grinding processes on the crystal surfaces.

The generated dihydrates before and after the 1st hydration cycle have been analyzed qualitatively using the XRD, as shown in Figure 10. The calcium sulfate dihydrate phase was the major component found in the diffractograms of all generated samples after hydration, as displayed in Figure 10. This indicates that the samples were well hydrated as no hemihydrate or anhydrite phases were discovered.

Table 2: Physical properties of pure β-HH and β-HH after the first cycle.

Sample name	d_{10} (μm)	d_{50} (μm)	d_{90} (μm)	BET surface area (m^2/g)	W/S ratio
β-HH	4.48	20.98	94.70	10.29	0.8
β-HH-1st cycle	1.80	8.18	135.90	11.86	1

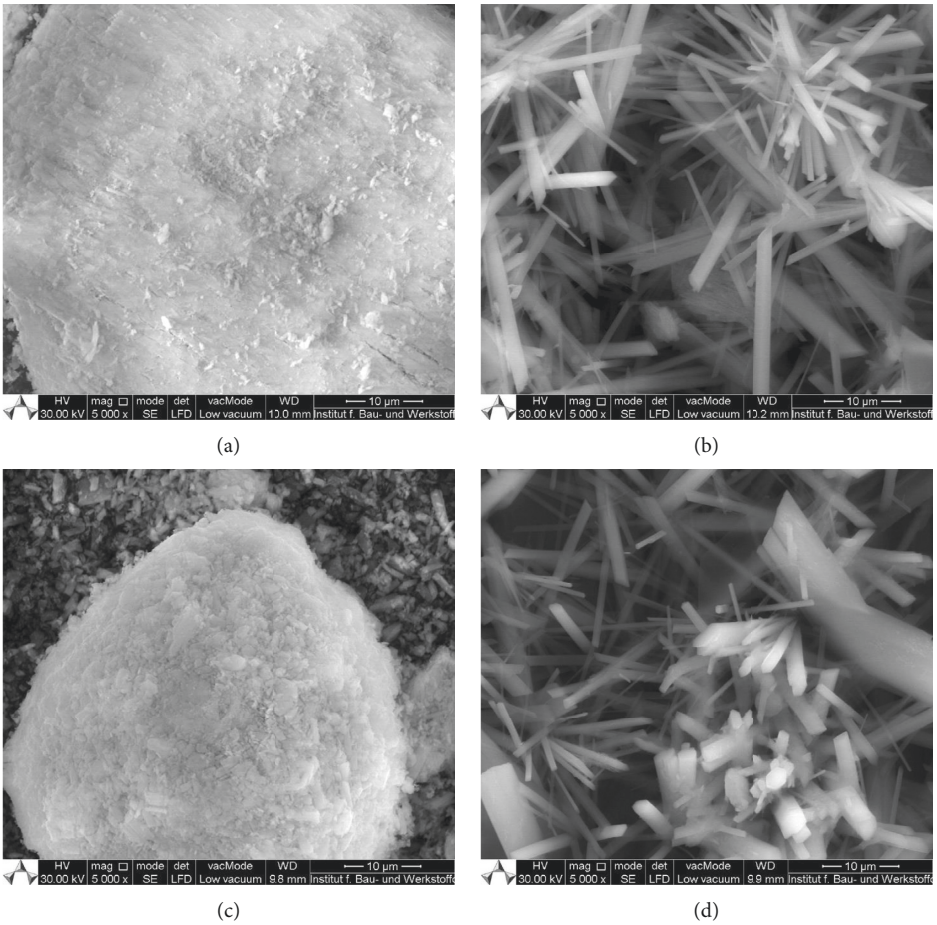

Figure 5: SEM images pure β-HH and β-HH after the first cycle before and after hydration: (a, b) pure β-HH before and after hydration, respectively, and (c, d) β-HH after the first cycle before and after hydration, respectively.

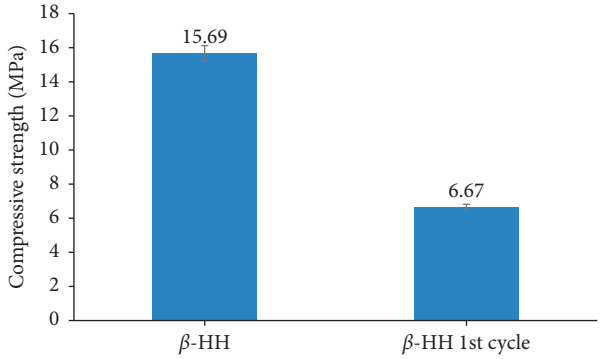

Figure 6: The compressive strength of the β-HH and β-HH after the first cycle.

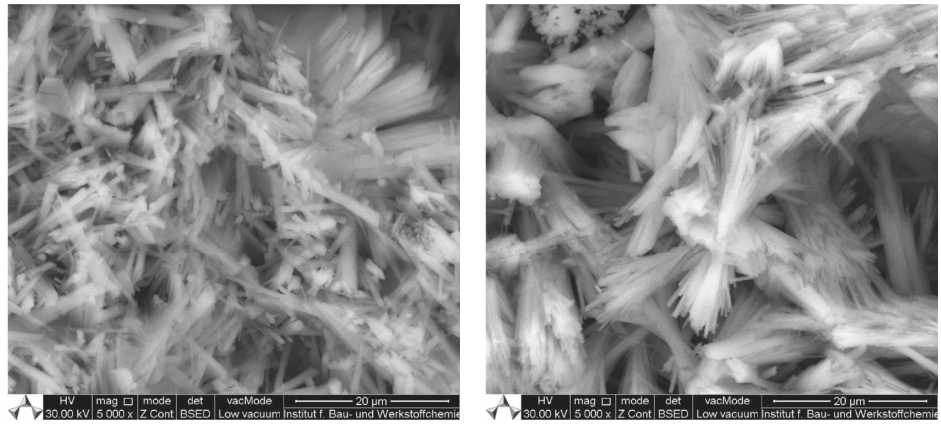

(a) (b)

Figure 7: SEM images for dihydrate crystals formation from β-HH and β-HH after the first cycle.

Table 3: Physical properties of pure SA α-HH and SA α-HH after the first cycle.

Sample name	d_{10} (μm)	d_{50} (μm)	d_{90} (μm)	BET surface area (m^2/g)	W/S ratio
SA α-HH	6.30	70.88	192.30	1.28	0.35
SA α-HH 1st cycle	2.12	19.79	270.36	7.06	0.90

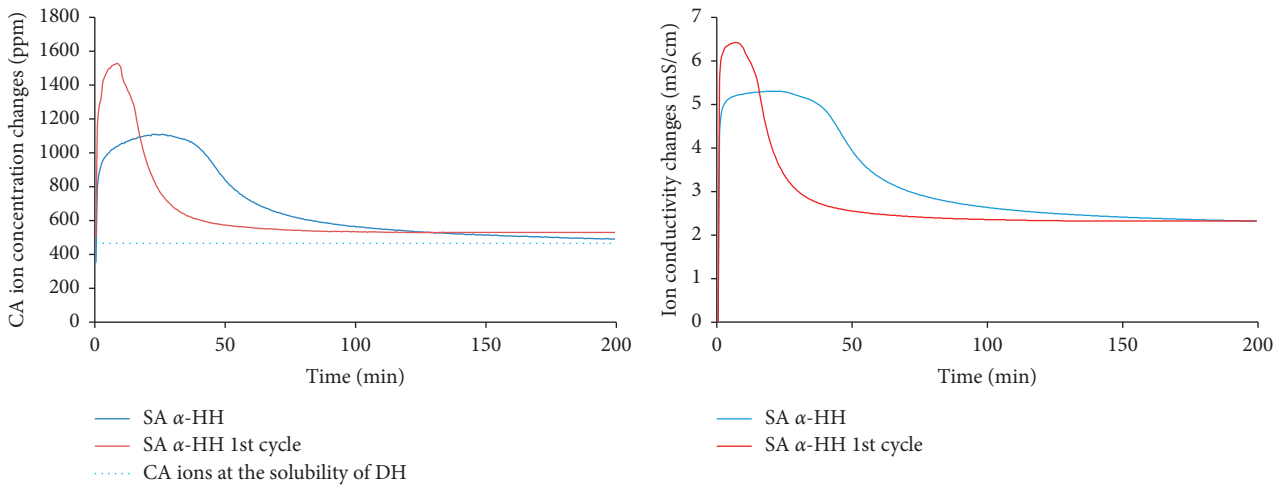

(a) (b)

Figure 8: Ca^{2+}-Ion concentration and ion conductivity changes for pure SA α-HH and SA α-HH after the first cycle: (a) ion concentration changes and (b) ion conductivity changes.

However, the intensity of the peaks differs slightly in length and positions. A similar result was obtained in the investigations by Rabizadeh et al. [39]. The DSC signals of the generated dihydrate indicate the phase transformation from dihydrate to soluble anhydrite through a two-step dehydration process of $CaSO_4 \cdot 2H_2O \longrightarrow CaSO_4 \cdot 0.5H_2O \longrightarrow \gamma CaSO_4$ as displayed in Figure 11 [6]. Moreover, the TG curves are compatible with the theoretical stochiometric percentage mass loss of water (21%). For instance, the generated dihydrate crystals form β-HH before and after the 1st hydration cycle, as shown from SEM images in Figure 7, can be confirmed by STA and XRD results.

From the SEM image, as shown in Figure 12, the high influence of the grinding process on the crystal morphology generates very fine particles with a large number of defects. Therefore, the hydration rate after the first reaction cycle increased. Due to this change in the microstructure of hemihydrate, which was generated after the recycling of SA α-HH, the compressive strength fails.

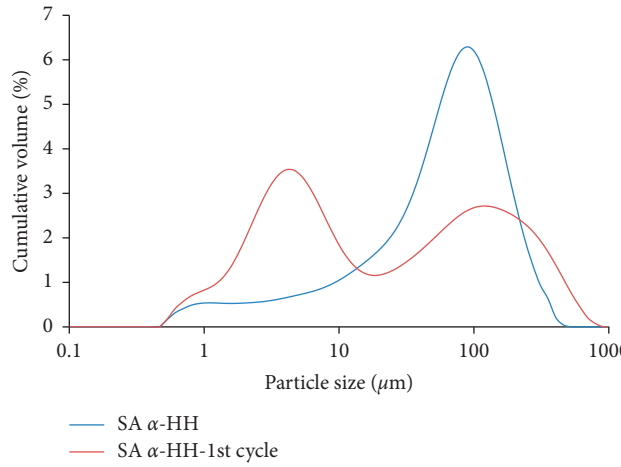

Figure 9: Particle size distribution of pure SA α-HH and SA α -HH after the first cycle.

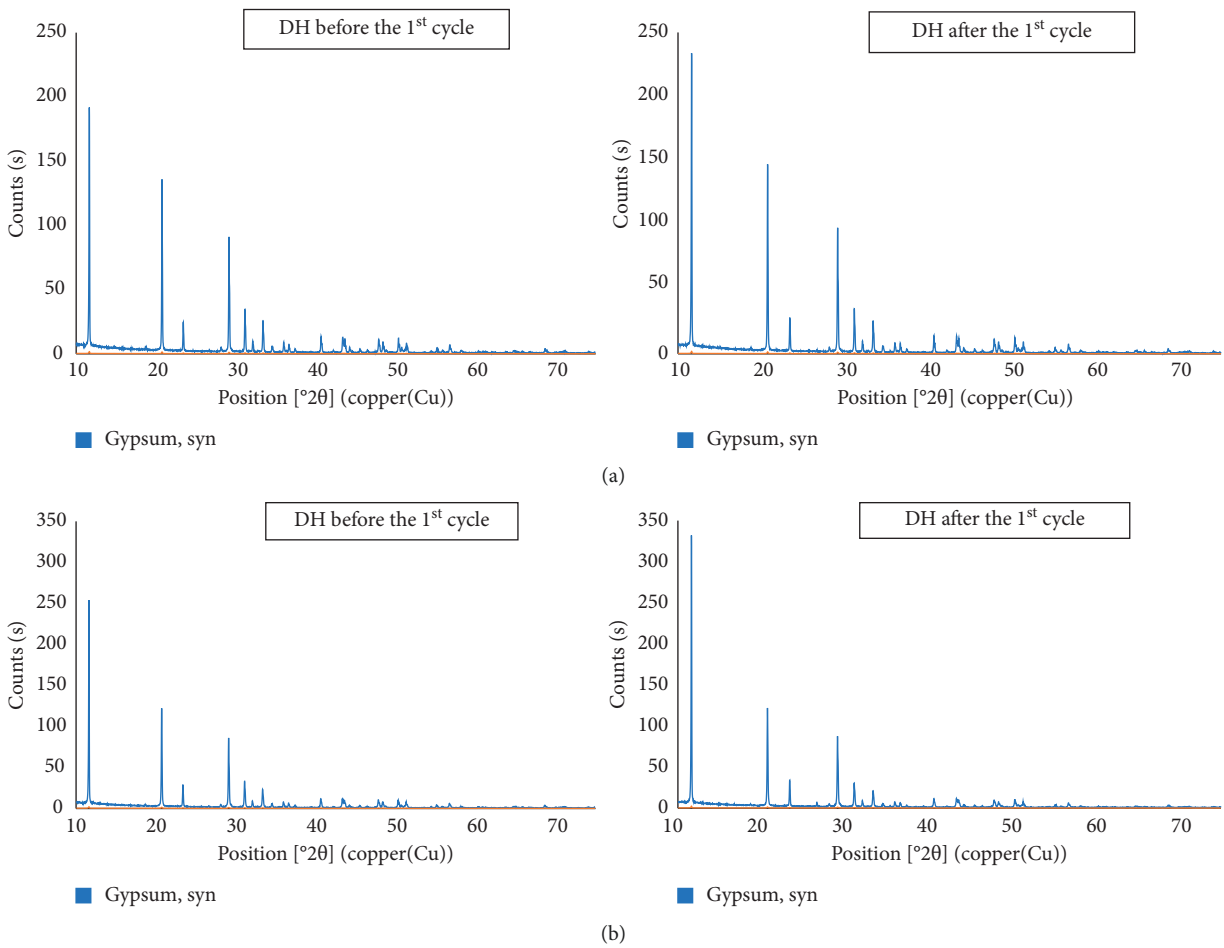

Figure 10: XRD patterns for the generated DH before and after the first hydration cycle from (a) β-HH and (b) α-HH.

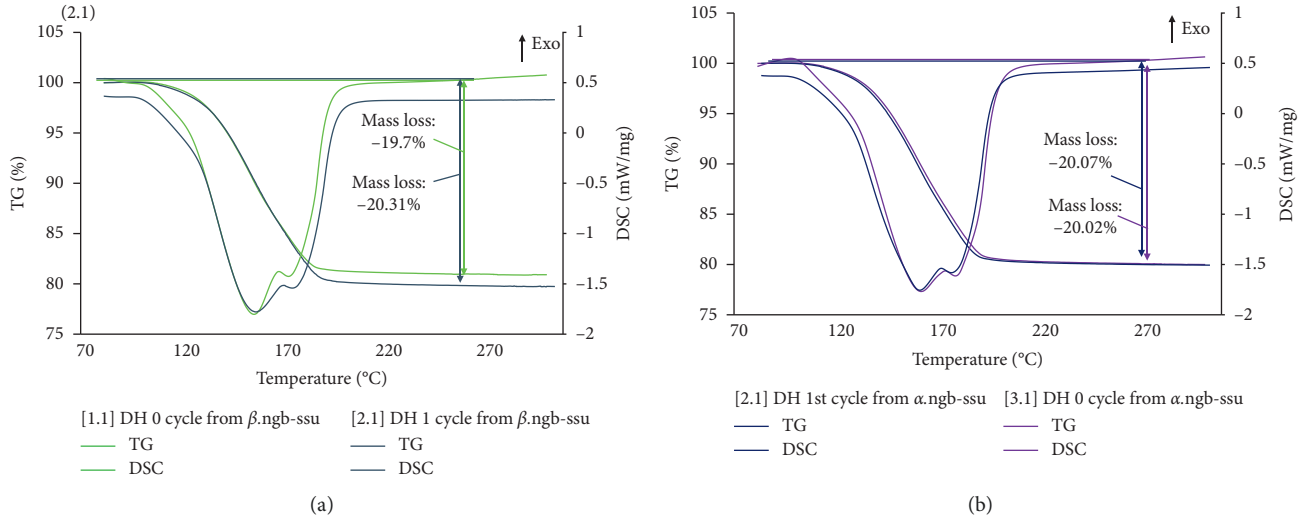

Figure 11: STA for the generated DH before and after the first hydration cycle from (a) β-HH and (b) α-HH.

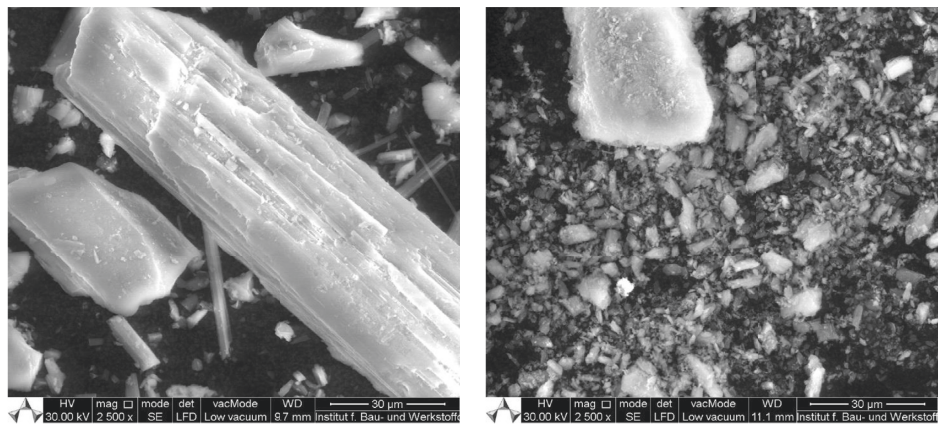

Figure 12: SEM images pure: (a) SA α-HH and (b) SA α-HH after the first cycle.

3. Conclusion

One of the major findings from this study was that the properties of the generated hemihydrate and dihydrate after the 1st reaction cycle were based on several factors such as type (α- or β-), purity, and properties of the hemihydrate in addition to the calcination mechanism and grinding procedure. The hydration rate of the recycled hemihydrate was varied due to the variation between the physical properties between the original hemihydrate and hemihydrate after the 1st reaction cycle. The differences in the mechanical properties of the formed dihydrate before and after cycling were based on several factors such as HH crystal size, HH surface area, water to hemihydrate ratio, pores generation during the drying process after hydration, the packing density, and the dihydrate crystal morphology. The grinding step of the recycled material decreases the particle size, increases the surface area, and changes the microstructure. The finer the particle size, the higher the amount of the required water to perform better workability leading to a decrease in the compressive strength of the recycled hemihydrate. Grinding also leads to high surface defects on the crystals, which impacts the setting time and the microstructure of the recycled hemihydrate. With an increase of the surface area of the hemihydrate, the water demand and the maximum reached ion concentration in the reaction solution increase, which leads to more seed crystals formation. Because of that process, the dihydrate crystals get smaller, and the number of branches increases. On the basis of the obtained results of this study, the particle size, surface area, and surface morphology of the starting material of hemihydrate are very important which is altering the properties of hemihydrate during the recycling process. The recycled calcium sulfate hemihydrate has to be taken as a new resource with its own characteristics and special impurities. The reveled result of this study is significant for the normal production of beta hemihydrate from the natural or FGD-gypsum. For better results, the repetition of the recycling process is

recommended in order to improve the properties of the recycled material after several reaction cycles. Investigations of the following cycle steps are needed to understand the mechanism in detail and to prove if there is a limit in the surface increase of hemihydrate and dihydrate.

Data Availability

The data that support the findings of this study are available from the corresponding author upon request.

Conflicts of Interest

The authors declare that they have no conflicts of interest.

References

[1] K. Gupta, S. Singh, and M. S. R. Rao, "Direct and facile room-temperature synthesis of nanocrystalline calcium sulfate dihydrate (gypsum)," *Crystal Growth & Design*, vol. 16, no. 6, pp. 3256–3261, 2016.

[2] G. Camarini, M. C. C. Pinto, A. G. d. Moura, and N. R. Manzo, "Effect of citric acid on properties of recycled gypsum plaster to building components," *Construction and Building Materials*, vol. 124, pp. 383–390, 2016.

[3] R. H. Geraldo, S. M. M. Pinheiro, J. S. Silva et al., "Gypsum plaster waste recycling: a potential environmental and industrial solution," *Journal of Cleaner Production*, vol. 164, pp. 288–300, 2017.

[4] C. Zhu, J. Zhang, W. Yi, W. Cao, J. Peng, and J. Liu, "Research on degradation mechanisms of recycled building gypsum," *Construction and Building Materials*, vol. 173, pp. 540–549, 2018.

[5] H. C. F. Cordon, F. C. Cagnoni, and F. F. Ferreira, "Comparison of physical and mechanical properties of civil construction plaster and recycled waste gypsum from São Paulo, Brazil," *Journal of Building Engineering*, vol. 22, pp. 504–512, 2019.

[6] W. Lou, B. Guan, and Z. Wu, "Dehydration behavior of FGD gypsum by simultaneous TG and DSC analysis," *Journal of Thermal Analysis and Calorimetry*, vol. 104, no. 2, pp. 661–669, 2011.

[7] A. N. Christensen, M. Olesen, Y. Cerenius, and T. R. Jensen, "Formation and transformation of five different phases in the $CaSO_4$–H_2O system: crystal structure of the subhydrate β-$CaSO_4{\cdot}0.5H_2O$ and soluble anhydrite $CaSO_4$," *Chemistry of Materials*, vol. 20, no. 6, pp. 2124–2132, 2008.

[8] C. Pritzel, R. Trettin, and Y. Sakalli, "Investigation of the hydration of hemihydrate with microscopic methods," in *Proceedings of the 14th European Microscopy Congress*, Aachen, Germany, September 2008.

[9] P. S. Bardella and G. Camarini, "Recycled plaster: physical and mechanical properties," *Advanced Materials Research*, vol. 374–377, pp. 1307–1310, 2011.

[10] G. Camarini, S. M. M. Pinheiro, and K. Tannous, "Thermal analysis of recycled gypsum from construction and demolition waste," *Applied Mechanics and Materials*, vol. 260-261, pp. 977–980, 2012.

[11] Z. Li, K. Xu, J. Peng, J. Wang, X. Ma, and J. Niu, "Investigation on the deterioration mechanism of recycled plaster," *Advances in Materials Science and Engineering*, vol. 2018, Article ID 4791451, 8 pages, 2018.

[12] G. Azimi, V. G. Papangelakis, and J. E. Dutrizac, "Modelling of calcium sulphate solubility in concentrated multi-component sulphate solutions," *Fluid Phase Equilibria*, vol. 260, no. 2, pp. 300–315, 2007.

[13] T. N. Harrison, "Experimental VNIR reflectance spectroscopy of gypsum dehydration: investigating the gypsum to bassanite transition," *American Mineralogist*, vol. 97, no. 4, pp. 598–609, 2012.

[14] Y.-W. Wang, Y.-Y. Kim, H. K. Christenson, and F. C. Meldrum, "A new precipitation pathway for calcium sulfate dihydrate (gypsum) via amorphous and hemihydrate intermediates," *Chemical Communications*, vol. 48, no. 4, pp. 504–506, 2012.

[15] S. J. Wang, Q. Chen, Y. Li, Y. Q. Zhuo, and L. Z. Xu, "Research on saline-alkali soil amelioration with FGD gypsum," *Resources, Conservation and Recycling*, vol. 121, pp. 82–92, 2017.

[16] S. Marinković, A. Kostić-Pulek, V. Logar, and P. Trifunović, "Recycling of waste FGD gypsum recycling of waste FGD gypsum," in *Proceedings of the 32 International Conference of Slovak Society of Chemical Engineering*, Tatranské Matliare, Slovakia, May 2005.

[17] S. Inazumi, H. Sano, and M. Yamada, "Estimation of gypsum hemihydrate content in recycled gypsums derived from gypsum boards," *Journal of Material Cycles and Waste Management*, vol. 18, no. 1, pp. 168–176, 2016.

[18] Z. Li, J. Peng, and X. Qiu, "Effect of different ways of STPP retarder addition on properties of recycled gypsum," *Journal of Wuhan University of Technology-Materials Science Edition*, vol. 32, no. 5, pp. 1125–1131, 2017.

[19] Z. Li, K. Xu, J. Peng, J. Wang, X. Ma, and J. Niu, "Study on hydration and mechanical property of portland cement-blended recycled plaster materials," *Advances in Materials Science and Engineering*, vol. 2018, Article ID 2692347, 8 pages, 2018.

[20] A. Ahmed and M. H. E. Naggar, "Effect of cyclic loading on the compressive strength of soil stabilized with bassanite-tire mixture," *Journal of Material Cycles and Waste Management*, vol. 20, no. 1, pp. 525–532, 2018.

[21] G. L. Vieira, A. P. Trovão, and C. R. Teles, "Perspective of environmental sustainability with waste recycling plaster in construction," in *Proceedings of the 16th International Waste Management and Landfill Symposium*, Cagliari, Italy, October 2017.

[22] S. M. M. Pinheiro and G. Camarini, "Characteristics of gypsum recycling in different cycles," *International Journal of Engineering and Technology*, vol. 7, no. 3, pp. 215–218, 2015.

[23] A. A. Khalil, A. Tawfik, A. A. Hegazy, and M. F. El-Shahat, "Effect of some waste additives on the physical and mechanical properties of gypsum plaster composites," *Construction and Building Materials*, vol. 68, pp. 580–586, 2014.

[24] T. Hofelich, L. Wadsö, A. L. Smith, S. Hamid, and S. Rose Mulligan, "The isothermal heat conduction calorimeter: a versatile instrument for studying processes in physics, chemistry, and biology," *Journal of Chemical Education*, vol. 78, 2001.

[25] 2018 Mettler-Toledo international inc. all rights reserved. perfection™ comb ca combination electrode, https://www.mt.com/de/en/home/products/Laboratory_Analytics_Browse/pH/sensor_electrode/Ion-selective_Electrodes/Combined_ISEs/perfectION_Ca_BNC.html.

[26] Malvern Instruments Ltd, *Mastersizer 2000*, Malvern Instruments Ltd., England, UK, 2006.

[27] S. Brunauer, P. H. Emmett, and E. Teller, "Adsorption of gases in multimolecular layers," *Journal of the American Chemical Society*, vol. 60, no. 2, pp. 309–319, 1938.

[28] I. Odler, "The BET-specific surface area of hydrated Portland cement and related materials," *Cement and Concrete Research*, vol. 33, no. 12, pp. 2049–2056, 2003.

[29] M. Ermrich and D. Opper, *XRD for the Analyst: Getting Acquainted with the Principles*, PANalytical, Almelo, Netherlands, 2nd edition, 2013.

[30] R. F. Egerton, *Physical Principles of Electron Microscopy: An Introduction to TEM, SEM, and AEM*, Springer, New York, NY, USA, 3rd edition, 2008.

[31] R. McCaffrey, *Recycling of gypsum and hydration of hemihydrate in the presence of retarding agents and other additives*, C. Pritzel, E. Abu Zeitoun, Y. Sakalli, and R. Trettin, Eds., Institut für Bau- und Werkstoffchemie, Universität Siegen, Siegen, Germany, 2018.

[32] O. Henning and D. Knöfel, *Baustoffchemie: Eine Einführung für Bauingenieure und Architekten; mit 104 Tafeln und zahlreichen Übungsbeispielen*, Verlag Bauwesen, Berlin, Germany, 6th edition, 2002.

[33] I. Berdugo, E. Romero, M. Saaltink, and M. Albis, "On the behaviour of the Ca-SO_4-H_2O system," *Revista de la Academia Colombiana de Ciencias Exactas*, vol. 32, no. 125, pp. 545–557, 2008.

[34] A. Lancia, D. Musmarra, and M. Prisciandaro, "Measuring induction period for calcium sulfate dihydrate precipitation," *AIChE Journal*, vol. 45, no. 2, pp. 390–397, 1999.

[35] G. Cao, *Nanostructures & Nanomaterials: Synthesis, Properties & Applications*, Imperial College Press, London, UK, 2004.

[36] H. Hamm, H. J. Kersten, and R. Hueller, "25 years experience gained in the European Gypsum Industry with the use of FGD gypsum," *Cement International*, vol. 4, pp. 92–102, 2004.

[37] D. Marchon, U. Sulser, A. Eberhardt, and R. J. Flatt, "Molecular design of comb-shaped polycarboxylate dispersants for environmentally friendly concrete," *Soft Matter*, vol. 9, no. 45, p. 10719, 2013.

[38] Jazmín Consuelo Aboytes Contreras, *Multi-Method Approach to Study the Influence of Additives in Ternary Systems: Gypsum, Water and Impurities*, Clausthal University of Technology, Clausthal-Zellerfeld, Germany, 2014.

[39] T. Rabizadeh, C. L. Peacock, and L. G. Benning, "Carboxylic acids: effective inhibitors for calcium sulfate precipitation?" *Mineralogical Magazine*, vol. 78, no. 6, pp. 1465–1472, 2014.